nature neuroscience

Stimulus contrast modulates functional connectivity in visual cortex

Ian Nauhaus[1], Laura Busse[2], Matteo Carandini[2,3] & Dario L Ringach[1,4,5]

Neurons in visual cortex are linked by an extensive network of lateral connections. To study the effect of these connections on neural responses, we recorded spikes and local field potentials (LFPs) from multi-electrode arrays that were implanted in monkey and cat primary visual cortex. Spikes at each location generated outward traveling LFP waves. When the visual stimulus was absent or had low contrast, these LFP waves had large amplitudes and traveled over long distances. Their effect was strong: LFP traces at any site could be predicted by the superposition of waves that were evoked by spiking in a ~1.5-mm radius. As stimulus contrast increased, both the magnitude and the distance traveled by the waves progressively decreased. We conclude that the relative weight of feedforward and lateral inputs in visual cortex is not fixed, but rather depends on stimulus contrast. Lateral connections dominate at low contrast, when spatial integration of signals is perhaps most beneficial.

Neurons in primary visual cortex (area V1) receive input from the thalamus and from an extensive network of lateral connections. The relative strength of these two signals remains controversial. One view holds that the responses of V1 neurons are largely determined by local processing of thalamic inputs[1–5], whereas another view states that V1 responses are substantially shaped by long-range lateral connections[6–13]. An implicit assumption in this debate has been that the relative weight of feedforward and lateral connectivity signals is fixed and is independent of the stimulus. We hypothesized that experimental findings supporting one or the other view could be reconciled if this relative weight was dependent on stimulus conditions.

To test this idea, we simultaneously recorded spiking activity and LFPs from multi-electrode arrays that were implanted in primary visual cortex in monkeys and cats. The LFP reflects the membrane potential of a local population of neurons. By computing spike-triggered LFP averages[14], we assessed the strength of postsynaptic activity at one cortical site that was caused by spiking at another location. Hence, this postsynaptic activity is a measure of functional connectivity between the site where the spikes are recorded and the site where the LFP is measured.

The LFP, especially in the absence of a sensory stimulus, is a highly variable signal characteristic of ongoing activity. We found that this activity was the result of the superposition of a myriad of traveling waves, each originating from spikes in a region spanning millimeters of cortex. Spikes at any given site generated a radial traveling wave of LFP activation representing net depolarizing synaptic input, whose amplitude decreased with distance. When the stimulus was absent, these lateral contributions extended over a large area and strongly influenced cortical activity, allowing us to predict the waveform of the spontaneous LFP traces with reasonable accuracy.

As the contrast of the visual stimulus increased, both the spatial footprint of lateral connectivity and its effect on visual responses were progressively reduced. These findings indicate that the relative weight of feedforward and lateral inputs is not fixed, but is contrast dependent. Our results offer a new conceptual framework that could help reconcile two views of cortical processing that have previously been believed to be incompatible.

RESULTS

We recorded spike activity and LFPs across 10 × 10 arrays of electrodes that were implanted in primary visual cortex of anesthetized monkeys (area 17) and cats (area 18). Previously, we established that the LFP represents a measure of local postsynaptic activity in a ~250-μm radius of the recording site[15]. Thus, sampling 400-μm intervals allows for estimates of postsynaptic activity in neuronal populations that are largely nonoverlapping.

To investigate how the spiking activity at one cortical site evoked synaptic input at another site, we calculated spike-triggered LFPs[14] (**Fig. 1a**). First, we selected an electrode as the reference site for the spiking activity (**Fig. 1a**). Then, we computed spike-triggered averages of the LFP signals across the entire electrode array (**Fig. 1a**). The spike-triggered LFP average was analyzed to estimate its peak (negative) amplitude and the time to peak relative to the generating spike (**Fig. 1b**). This procedure was repeated by selecting all possible reference electrodes in the array.

Cortical spikes trigger traveling waves of LFP activity

We first characterized spike-triggered LFPs during spontaneous activity and found that spikes at any given electrode site created outward

[1]Biomedical Engineering Department, University of California Los Angeles, 405 Hilgard Avenue, Los Angeles, California 90095, USA. [2]Smith-Kettlewell Eye Research Institute, 2318 Fillmore Street, San Francisco, California 94115, USA. [3]UCL Institute of Ophthalmology, University College London, 11-43 Bath Street, London EC1V 9EL, UK. [4]Departments of Neurobiology and [5]Psychology, University of California Los Angeles, 405 Hilgard Avenue, Los Angeles, California 90095, USA. Correspondence should be addressed to I.N. (inauhaus@gmail.com).

Received 20 June; accepted 20 October; published online 23 November 2008; doi:10.1038/nn.2232

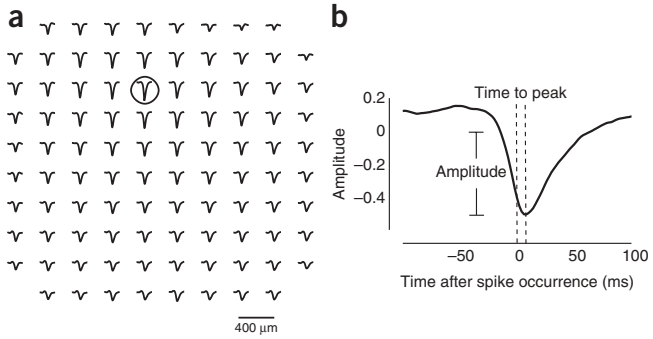

Figure 1 Spike-triggered LFPs as a measure of functional connectivity. (**a**) The spike-triggered average of the LFP signal at different locations in the array is shown. The array consisted of a 10 × 10 array of electrodes, but the corners were not wired, resulting in 96 active electrodes. Grid separation was 400 μm between adjacent electrodes. In this example, reference spikes originated from the electrode that is indicated by the circle. The spike-triggered LFP average across the entire array is shown by the traces. The calculation of spike-triggered LFPs was repeated for all possible reference locations. (**b**) Measurements of the spike-triggered LFP. For each spike-triggered LFP average, we computed two parameters: the maximum peak (negative) deflection and the time at which it peaked. From these data, we analyzed how the amplitude and time to peak depended on the cortical distance between the reference spike location and the target LFP location.

propagating waves of LFP activity across the cortex. The time to peak increased linearly with radial distance as $\frac{d}{v}$, where d represents the cortical distance and v is the propagation speed (**Fig. 2**). This propagation speed was, on average, 0.24 ± 0.20 m s^{-1} in monkeys and 0.31 ± 0.23 m s^{-1} in cats (mean ± s.d.). The propagating wave that we observed following cortical spikes is reminiscent of the spread of activity that has previously been reported in response to a small visual stimulus[8,16–18]. This spread of activity constitutes a traveling wave that propagates at ∼0.3 m s^{-1} in cats[17] and at 0.09–0.25 m s^{-1} in monkeys[18]. These speeds of propagation suggest that the activity may travel along long-range horizontal connections[19], whose propagation speed in cats is ∼0.3 m s^{-1} (ref. 20).

The peak amplitude of these radial waves decayed with distance from the spikes in an approximately exponential manner, $M \exp\left(\frac{-d}{\lambda}\right) + B$, where M is the magnitude of the wave (**Fig. 2**). The space constant λ captures the rate at which the amplitude falls off with distance; during spontaneous activity, it averaged 2.1 ± 0.6 mm for monkeys (mean ± s.d., n = 99 sites) and 5.8 ± 1.9 mm for cats (n = 116 sites). The parameter B represents an asymptotic baseline amplitude achieved at large cortical distances.

The tight temporal correspondence of the spikes and the waves, the linear dependence of wave delay on cortical distance, and the temporal asymmetry of the correlations suggest that the spikes caused the LFP waves. Temporal asymmetry refers to the fact that a spike at location A correlates with a delayed LFP response at location B, whereas a spike at location B correlates with a delayed LFP response at location A. A fixed common input to locations A and B would not be able to generate this asymmetric temporal pattern of correlations.

Predicting the LFP from the spiking of neuronal populations

To further test the causal relationship between spikes and LFP waves, we asked whether the LFP signal at one site could be predicted from spiking at remote locations. This is a demanding test, as the LFP in the absence of a stimulus is a highly variable signal and, to the best of our knowledge, no computational model has succeeded in predicting it quantitatively.

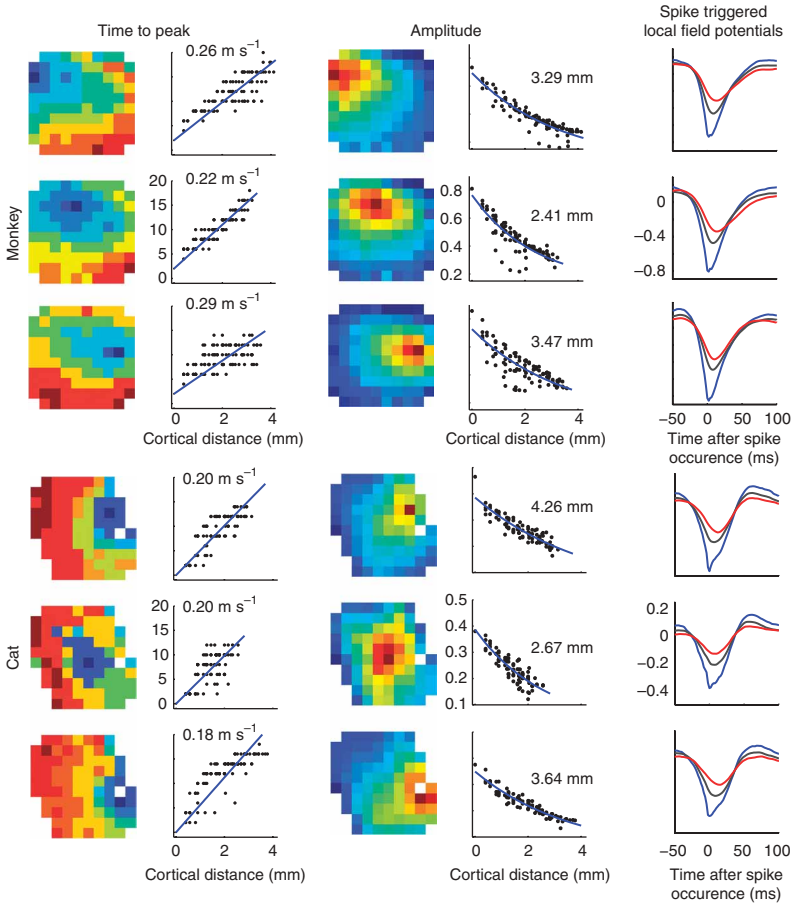

Figure 2 Spikes initiate traveling waves of LFPs in the cortex. Examples are shown from one array that was implanted in monkey V1 (top) and one penetration in cat V1 (bottom). Each row depicts data from the spike-triggered LFPs from a single spiking location. Left, the dependence of time to peak as a function of cortical distance from the triggering electrode is shown, both as an image (left) and as a scatter plot (right). Middle, the amplitudes of the signals are shown in a pseudo-color map to the left (the location of the reference spike corresponds to that of the darkest red–saturated pixel) and scatter plots of amplitude versus distance obtained by re-plotting the data are shown on the right. Estimated space constants appear at the inset. Estimated propagation velocities appear at the inset. Right, curves representing average LFP waveforms at three different distances from the location of the reference spikes are shown. The blue curve is the waveform at the spike location. The gray curve is the average waveform at distances of ≥400 μm and <2,400 μm, and each red curve is the average at a distance of ≥2,400 μm and <3,600 μm. The dependence of magnitude and time to peak are evident in these average curves.

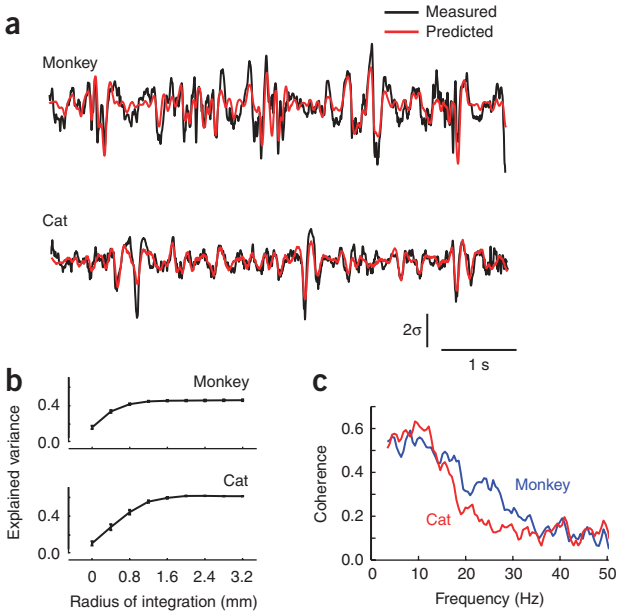

Figure 3 Predictions of LFPs from the spiking activity across a neuronal population. (**a**) Predictions for the LFP were generated on the basis of the linear superposition of the traveling waves induced by spikes across the entire array. Shown here are two examples of measured (black) and predicted (red) LFPs at one site in a cat and monkey. The vertical bar represents 2 s.d. of the LFP. (**b**) The predictions improved as the integration region, centered on the target LFP location, increased. The maximum amount of variance accounted for saturated for regions over ~1.2 mm in radius. Error bars represent ± s.e.m. (**c**) Predictions best captured the low temporal-frequency components of the LFP. The graph shows the coherence between measured and predicted responses in the monkey and cat. Coherence was largest in the band between 2 and 15 Hz and decreased steadily to reach a baseline level at ~35 Hz.

We found that the waveform of the LFP signal measured during spontaneous activity can in fact be well predicted given knowledge of the individual spike times across the array (**Fig. 3a**,**b**). Having chosen an arbitrary site for measuring the LFP, we computed the average spike-triggered waveforms from spikes at each remaining site in the array. Superposition of these waves on the basis of the actual spike times at these sites yielded a simple linear prediction of the LFP trace. This prediction was markedly accurate (**Fig. 3a**) and the accuracy increased as the area over which the spikes were integrated extended to encompass a larger cortical region (**Fig. 3b**). The improved accuracy obtained by summing from distal sites is further evidence against a single common input to the entire area, as the contributions from increasingly distant sites arrive with correspondingly increasing delay. On average, linear superposition accounted for 46% of the LFP variance in monkeys and 51% of the variance in cats (**Fig. 3b**), with the residual being largely restricted to high temporal frequencies (**Fig. 3c**).

These results indicate that the synaptic input to a local region during spontaneous activity is largely explained by the effect of spikes at distal cortical locations. Specifically, the synaptic input to neurons during spontaneous activity can be thought of as the superposition of a myriad of traveling waves originating from individual spikes distributed over an extended region of cortex.

Lateral connectivity depends on preferred orientation

Lateral connectivity in visual cortex is thought to be related to maps of orientation preference. Anatomical studies indicate that horizontal connections have a tendency to privilege sites with similar orientation preference[18,21]. Imaging studies, accordingly, suggest that activity at sites with similar orientation preference may be more strongly correlated[9,10].

We therefore asked whether the traveling waves showed a bias toward sites with similar orientation preference (**Fig. 4**). We first accounted for the strong dependence on cortical distance by subtracting the exponential fits from the data points corresponding to each reference electrode. The residual amplitudes measured at each site were then z scored and plotted as a function of the absolute difference in orientation preference between the site and the reference location. Orientation preference at each site was computed by reverse correlation in the orientation domain[6]. The population data showed a significant effect of orientation on functional connectivity, whereby sites with similar orientation preference were linked more strongly than those with orthogonal preferences (t test, $n - 2$ degrees of freedom, $P < 2 \times 10^{-7}$; **Fig. 4**). When tested individually on each animal, we found that the effect was statistically significant in three of the four animals (cats and in one monkey, $P < 0.002$; one monkey, $P = 0.82$).

Thus, our results are largely consistent with those of prior studies. The differences in the overall magnitude of the effect may be a consequence of the different measures that were used, LFPs rather than voltage sensitive–dye signals. Because of the different spatial scales of the orientation maps in the two species, it is perhaps not surprising that the effect was harder to detect in monkeys. Orientation preference maps in monkeys have smaller periodicity than in cats, and thus the effect of orientation could be overwhelmed by the strength of the effect of cortical distance.

Lateral connectivity depends on contrast

The phenomena discussed so far concern spontaneous activity, that is, the ongoing activity measured in the absence of visual stimulation. These phenomena were profoundly modified by the introduction of a strong visual stimulus (**Fig. 5**). We measured spikes and LFP traces during the presentation of a set of full-field drifting gratings at 100% contrast. We computed spike-triggered LFPs for this driven activity with the same methods that we employed in the analysis of spontaneous activity. First, the amplitudes of the spike-triggered LFPs were much smaller during driven activity than during spontaneous activity (**Fig. 5**). There was, therefore, a global tendency for the cortex to

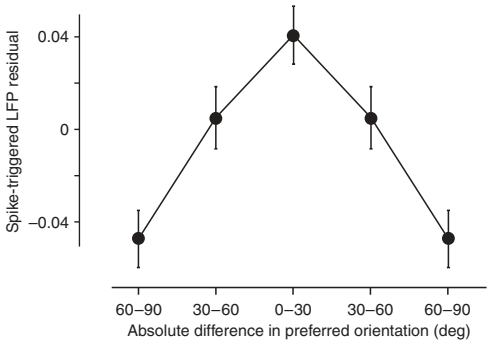

Figure 4 Sites with similar orientation preference are more strongly linked than sites with dissimilar orientation preference. The abscissa represents the absolute difference in orientation between the reference site and the site of the spike-triggered LFP. The ordinate corresponds to residual z-score values of the amplitude after subtracting the distance dependence predicted by the exponential fits. Plotted are the mean and standard error bars for three different bins of orientation difference. Two of the bins were plotted twice to make the curve symmetric solely for presentation purposes.

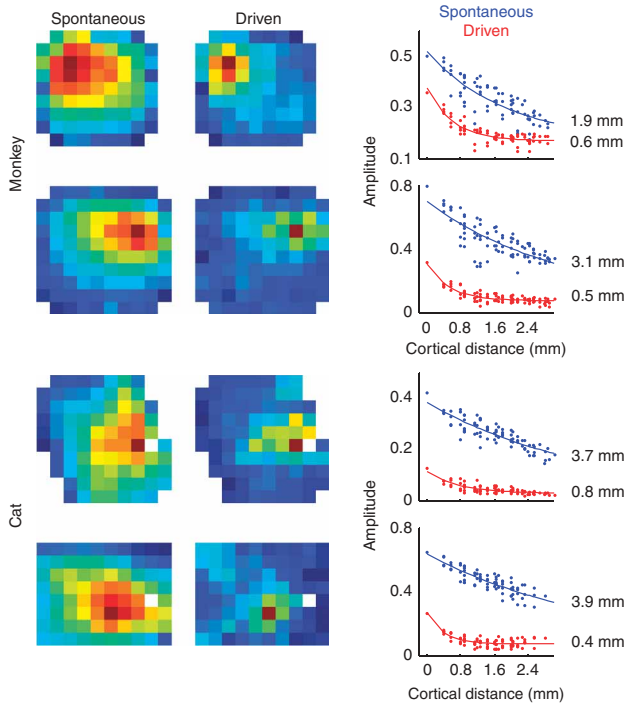

Figure 5 Visual stimulation modifies the effective lateral connectivity in the cortex. Each row shows the dependence of the spike-triggered LFP amplitudes as a pseudo-color image in spontaneous and driven conditions and as scatter plots. The top two examples correspond to two different monkeys. The bottom two are from two different cats. The solid curves in the scatter plot are best exponential fits to the data and the estimated space constants appear at the inset.

become decorrelated during strong visual stimulation relative to its spontaneous state. Second, there was a clear change in the shape of the fall-off function, with space constants in the driven condition being substantially smaller than those in the spontaneous condition. This reduction of the space constant indicates that the relative synaptic input to a given region became more spatially restricted at high contrast.

To quantify this stimulus-induced modulation of lateral connectivity, we computed ratios from parameters in the exponential fits: a ratio of space constants, $\frac{\lambda_{spont}}{\lambda_{driven}}$, and a ratio of magnitudes, $\frac{M_{spont}}{M_{driven}}$ (**Fig. 6a**). When comparing the spontaneous condition to the driven condition, space constants in both cats and monkeys decreased by a factor of 4.2 ± 2.4 (3.0 ± 2.3 in monkeys and 5.5 ± 2.1 in cats, geometric mean ± geometric s.d.), whereas the magnitudes decreased, on average, by a factor of 2.2 ± 1.9 (1.7 ± 1.8 in monkeys and 2.7 ± 1.9 in cats, in all cases a t test of the log-ratio yielded $P < 10^{-20}$).

The change in functional connectivity introduced by high-contrast visual stimulation represents an extreme of a gradual change seen with progressively stronger stimuli. In two monkeys, we collected data from drifting gratings at an intermediate contrast (25%) and found that the modulation of lateral connectivity depended smoothly on contrast (**Fig. 6b**).

As a control experiment, we repeated the analysis by triggering on the spikes of well-isolated single units rather than on those collected as multi-unit activity (**Fig. 7**). Indeed, an artifactual cause for the changes seen during visual stimulation would occur if visual stimulation changed the pool of neurons contributing to the multi-unit activity. The results that we obtained from single-unit activity were very similar to those that we obtained from multi-unit activity. The observed differences in spike-triggered LFPs space constants and magnitudes between spontaneous and driven conditions did not depend on the type of spike isolation (**Fig. 7**, compare with **Fig. 5**), providing further evidence that stimulus contrast modulates the strength and extent of lateral connectivity.

Along similar lines, we asked whether the change in functional connectivity induced by stimuli could be observed directly in the subthreshold responses, which are more directly related to synaptic inputs than spike trains (**Fig. 8**). We therefore studied the cross-correlations between LFP signals at pairs of sites. As expected, these cross-correlation functions did not show any evidence of traveling waves (the functions peaked at time zero independently of the distance between sites). Indeed, considerations of symmetry dictate that there is no reason why synaptic activity in one location of cortex should consistently precede activity in another location. The correlation functions, however, did show a clear weakening with increasing

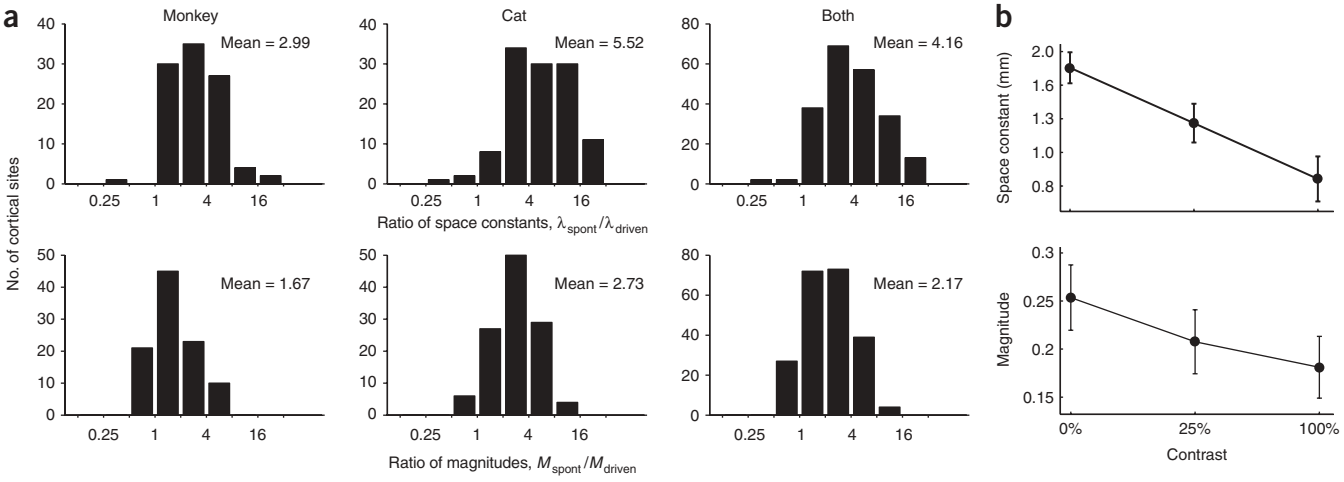

Figure 6 Effect of contrast on the magnitude and spatial extent of lateral interactions. (**a**) Histograms of the ratio of space constants $\frac{\lambda_{spont}}{\lambda_{driven}}$ (top) and the ratio of magnitudes $\frac{M_{spont}}{M_{driven}}$ (bottom). The effect was robust and similar in both monkeys and cats. The average ratio is shown at the inset of each histogram. (**b**) Smooth dependence on contrast. The plots show the mean values of the space constant and magnitude for three different contrast levels: 0 (spontaneous), 25 and 100% contrast. These represent the average behavior in two monkeys. Error bars represent ± s.e.m.

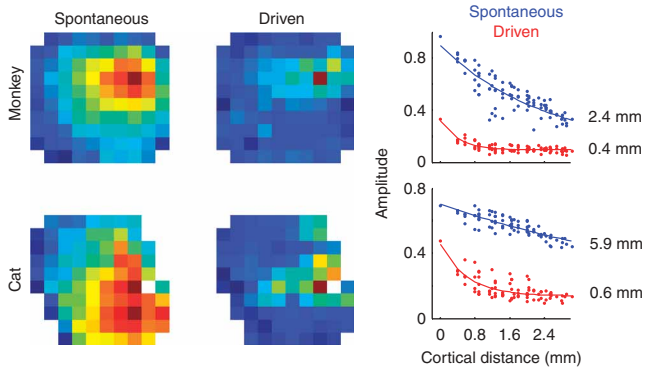

Figure 7 Results are unchanged by triggering on multi-unit or single-unit activity. In those cases where single-unit activity could be well isolated, we obtained results that were very similar to those obtained using multi-unit activity as the triggering events. The figure shows kernels obtained by triggering with well-isolated cells. These should be compared to those obtained with multi-unit activity in the middle panels of **Figure 5**.

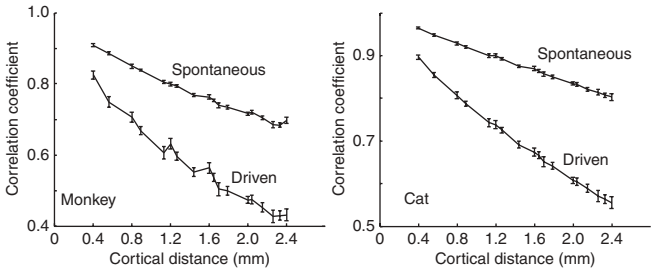

Figure 8 Correlation between pairs of LFP signals shows a contrast dependence that is similar to spike-triggered averaging of LFPs. The graphs depict the correlation coefficients between LFPs as a function of cortical distance for spontaneous and driven stimulus conditions. The correlation coefficients fell off more rapidly with cortical distance in the driven condition (100% contrast full-field drifting gratings) than in the spontaneous case. Error bars represent ± s.e.m.

contrast (**Fig. 8**), providing further evidence that increasing stimulus strength decouples cortical activity in space.

DISCUSSION

We measured spike-triggered averages of LFP signals across a cortical patch as a measurement of effective cortical connectivity. This analysis circumvents problems that are associated with spike cross-correlation measurements, such as the low probability of finding two cells with significant interactions[22,23] and the nonlinear dependence of correlation coefficients on the mean spike rate of the cells under consideration[24–26]. This method allowed us to study how lateral connectivity is modified when the stimulus contrast is changed without having to account for changes in feedforward processing between retina and cortex (such as changes in temporal delays with contrast). Furthermore, the technique enabled us to study lateral connectivity even in the absence of a visual stimulus.

We found that a spike induced a wave of LFP activity moving away from the spike location. A number of attributes of these traveling waves suggest that they propagate along long-range horizontal connections in visual cortex. First, similar to horizontal connections[19], the waves extended over a distance of millimeters. Second, similar to horizontal connections[20], the waves traveled at the relatively slow speed of $\sim$0.3 m s^{-1}. Third, similar to horizontal connections[18,21], the waves had a tendency to privilege sites with similar orientation preference.

Alternative explanations for the traveling waves, based on common input from outside V1, seem much less likely. In principle, our traveling waves could result from LGN inputs in two ways. First, there might be divergence of LGN afferents, with retinotopically corresponding areas receiving input before more distal areas. Second, there might be traveling waves in LGN itself, which would then be simply reflected in the responses of area V1. Both of these possibilities seem very unlikely given the results of experiments using LFP averages in V1 triggered by spikes in the LGN. First, the spatial spread of LFPs triggered from spikes in the thalamus and measured in V1 falls off with a space constant of $\sim$0.2 mm[14], smaller than what we observed by at least a factor of 10. Second, temporal delays in the LFP averages that are triggered by thalamic spikes differ by less than 100 µs across the V1 area that is being innervated (J.-M. Alonso and J. Jin, State University New York College of Optometry, personal communication; see also ref. 27), whereas our differential delays were 100-fold higher, on the order of tens of milliseconds. Finally, we ruled out traveling waves in the LGN by the dependence of the spike-triggered LFPs on relative orientation (**Fig. 4**).

Our observation of traveling waves caused by cortical spikes is consistent with prior studies that measured LFP[16] and membrane potential[8] responses in V1 neurons as a function of focal visual stimulation. These studies found an increase in the latency of depolarization that was triggered by a focal visual stimulus as the stimulus was moved away from the center of the receptive field under consideration. On the basis of our results, one can reinterpret these data by assuming that focal visual stimulation evoked local spiking activity in V1 that propagated, by means of horizontal connections, to the target neurons.

In addition to a systematic dependence of the time to peak on cortical distance, the spike-triggered LFP signal exhibited a nonzero response before the occurrence of the spike. This 'noncausal' response has also been noted in dual intracellular recordings, where the average membrane potential of one cell was triggered by the spikes of a nearby neuron[28]. Activity before the spike may be the result of contributions from various sources. A first source consists of correlation in space: common correlated input received by both cortical locations[28]. A second source consists of correlation in time: spiking at one location may by autocorrelated in time, and a wave that appears to originate from a given spike may in fact originate, in part, from a preceding spike. Indeed, when we corrected the spike-triggered LFPs by factoring out the autocorrelation of the spike train, the resulting traces were somewhat narrower in time, but peaked at the same time (**Supplementary Fig. 1** online), leading to a reduction of the noncausal signal at negative times. A third contribution may originate from the band-limited nature of the LFP signal and its characteristic $1/f$ spectrum, which would prevent the spike-triggered LFP from showing sharp transients.

The progressive disappearance of the traveling waves as the contrast was increased indicates that the relative balance between feedforward and lateral signals is not a fixed quantity, as has been previously assumed. Both the magnitude and the spatial extent of lateral interactions in visual cortex increased markedly as stimulus contrast was reduced, being maximal at zero contrast. This finding promises to reconcile two apparently opposite views: the view that the responses of V1 neurons are largely determined by local processing of thalamic inputs[1–5] and the view that V1 responses are substantially shaped by long-range lateral connections[6–13,29].

These effects of contrast on lateral connectivity are consistent with studies of spatial integration in single neurons that found decreased spatial summation at higher contrast levels[12,30–32]. On average, these studies found a threefold change in the scale of spatial summation,

which is comparable to the average change that we observed in the space constant (**Fig. 6a**). Future measurements using similar techniques could indicate whether the lateral interactions that we have observed are sufficient to explain the reported changes in spatial summation.

The effects of contrast that are revealed by our results are also consistent with a number of additional, previously disconnected observations. First, the strength of traveling waves elicited in V1 by focal visual stimuli is markedly reduced when those stimuli are embedded in large, high-contrast patterns[16]. Second, increasing contrast reduces the correlated response variability among pairs of nearby neurons in macaque V1 (ref. 33). Finally, increasing contrast decreases the trial-to-trial variability of membrane potential responses in cat V1 (ref. 34), suggesting that there is a decreased role of intracortical connections.

The finding that the effectiveness of lateral connectivity depends heavily on contrast suggests that there might be a relationship between lateral connectivity and the many phenomena of contrast gain control that have been observed in cortex. Perhaps increasing the effectiveness of lateral connectivity acts to increase cortical amplification, whereas decreasing it would decrease cortical amplification. This scenario predicts that the effectiveness of lateral connectivity, spatial summation and cortical gain must necessarily be linked to one another.

A recent study relying on voltage-sensitive dye imaging of primary visual cortex reported that spatial correlations in V1 are independent of stimulus contrast[35], whereas our results using correlations between LFP signals show a clear effect of contrast (**Fig. 8**). There are a few reasons for this apparent discrepancy. First, the stimuli used in these two studies differed considerably; we used large stimuli, whereas the prior study used localized Gabor patches. When using a localized Gabor patch, cortical areas surrounding the stimulus are likely to be in a state that is not very different from the spontaneous regime and the effect of lateral interactions may not be affected much by varying the contrast of the stimulus. Second, our contrast levels ranged from 0% (spontaneous) to 100%, whereas the comparisons of the prior studies were carried out on the basis of a smaller range of 7% and 25% contrast.

The exact cellular and network mechanisms that are involved in modulating lateral connectivity are unknown and require further study. One conjecture, based on a computational model of spatio-temporal integration, is that increases in background synaptic activity can reduce the spatial scale of integration in the dendritic tree by a factor of 3 to 5 (refs. 36,37), a prediction that compares well with the magnitude of our effects. Another possibility, suggested by measurements *in vitro*, is that a weak stimulus will only recruit excitatory horizontal signals, but a strong stimulus may also recruit di-synaptic inhibitory signals[20,38].The interaction between the two signals may result in an effective decrease in lateral coupling as the stimulus contrast increases.

Our findings demonstrate that the relative weight of feedforward and lateral inputs is determined, at least in part, by the strength of the visual stimulus. The stronger the visual stimulus, the more the system will work in a feedforward mode, where local signals are faithfully processed and transmitted by the cortical population. When the visual stimulus is weak, the system attempts to integrate information across visual space, and therefore relies more on cortical network interactions[21]. This suggests that the role of intra-cortical connectivity would be best revealed when using weak stimulation[39]. Conversely, high-contrast stimuli would be expected to drive the local circuitry into a feedforward mode. Our findings, therefore, suggest that two apparently incompatible views of cortical processing may represent the ends of operating regimes that are largely determined by the strength of the sensory input.

METHODS

Animal preparation. The main data reported here were obtained in two cats and two monkeys (data from an additional monkey and cat are shown in **Supplementary Fig. 2** online). Experiments were conducted according to the Guidelines for the Care and Use of Mammals in Neuroscience and Behavioral Research from the US National Institutes of Health.

Experiments in monkeys were conducted at the University of California Los Angeles under the supervision of the Chancellor's Animal Research Committee. Young adult monkeys (*Macaca fascicularis*, 3.2–4.2 kg) were sedated with acepromazine (30–60 μg per kg of body weight), anesthetized with ketamine (5–20 mg per kg, intramuscular) and then anesthetized again with isofluorane (1.5–2.5%, vol/vol). An endotracheal tube was inserted to allow artificial respiration. All surgical sites were infused with local anesthetic (2% xylocaine, wt/vol, subcutaneous). After this initial surgery, the anesthesia was switched to a combination of sufentanil (0.05–0.2 μg per kg per h) and propofol (2–6 mg per kg per h).

Experiments in cats were conducted at the Smith-Kettlewell Eye Research Institute under the supervision of the Institutional Animal Care and Use Committee. Young adult cats (2–4 kg) were anesthetized first with ketamine (22 mg per kg, intramuscular) and xylazine (1.1 mg per kg, intramuscular), and then with sodium penthotal (0.5–2 mg per kg per h, intravenous) and fentanyl (typically 10 μg per kg per h, intravenous), supplemented with inhalation of N_2O (typically a 70:30 ratio with O_2). Cats received an anticholinergic agent (atropine sulfate, 0.05 mg per kg, intramuscular, daily) and the nictitating membranes were retracted with topical phenylephrine.

Pupils were dilated with ophthalmic atropine and gas-permeable contact lenses were fitted to protect the corneas. Eye movements were prevented by a neuromuscular blocker, pancuronium bromide (0.10 mg per kg per h in monkeys, 0.15 mg per kg per h in cats), that was administered after surgical procedures were complete.

To ensure a proper level of anesthesia throughout the duration of the experiment, we continuously monitored rectal temperature, heart rate, end-tidal CO_2, airway pressure and electroencephalography (via a neonatal monitor in monkeys and a veterinary monitor in cats). In monkeys, we also measured noninvasive blood pressure, urine output and urine-specific gravity (every 4–5 h to ensure adequate hydration). Drugs were administered in balanced physiological solution to deliver a fluid volume of 5–10 ml per kg per h. Rectal temperature was maintained near 38.0 °C in cats and near 37.5 °C in monkeys. Expired CO_2 was maintained at near 4.3% in cats and at near 5.0% in monkeys by adjusting the stroke volume and ventilation rate of a respiration pump. Animals were administered a broad-spectrum antibiotic (in monkeys, we used bicillin at 50,000 injectable units per kg, administered every other day; in cats, we used cephazolin at 20 mg per kg intramuscular, administered twice daily) and anti-inflammatory steroid (dexamethasone, 0.5 mg per kg every other day in monkeys and 0.4 mg per kg daily in cats).

Electrophysiology and visual stimulation. We implanted a 10 × 10 electrode array (400-μm separation and 1.5-mm electrode length) in area V1. In cats, V1 includes both areas 17 and 18, and we placed the electrodes in area 18 because of its accessibility from the surface of the brain. To avoid excessive cortical damage, the arrays were inserted at high speeds (around 8 m s^{-1}) using a pneumatic insertion device. Insertion depths were about 0.8–1 mm. Although we lack histological confirmation, most of our recordings probably originated in the superficial layers of the cortex. The array and surrounding tissue was covered in 1.5% agar to improve stability.

A Cerebus 128-channel system (Cyberkinetics) was used to sample the data. In each channel, we set thresholds to ~4 s.d. of the background noise. Threshold crossing were considered to be multi-unit activity and were pooled together to trigger the averaging of LFPs at other locations. The average firing rate of multi-unit activity in the spontaneous condition was 20 spikes per s, whereas we obtained rates of 80 spikes per s at 100% contrast. LFP signals were sampled at 2 kHz with a wide-band front-end filter (0.3–500 Hz). We further digitally filtered them using an eighth-order high-pass Butterworth filter with a cutoff of 3 Hz and a tenth-order low-pass Butterworth filter with a cutoff at 90 Hz. After filtering, the signals for each channel were independently *z* scored. The spike-triggered average of the LFPs was carried out on these normalized signals (in absolute terms, the amplitude peak of the LFP triggered at the same

electrode was ~12 μV on average). In the spontaneous condition, the animals were looking at a uniform screen of the same mean luminance as in the driven condition. In the driven condition, the animals were shown drifting gratings at one fixed orientation (total of 40-s stimulation). For each electrode, the orientation that generated the largest response was used. The spatial and temporal frequency of the grating was set to drive most of the cells isolated by the array and was fixed across the experimental conditions. The stimulus was large (at least 10 × 10 degrees of visual angle) and the receptive fields were located near the center of the patch. The typical overlap of receptive fields across the array in a couple of these experiments is shown in **Supplementary Figure 2**. In addition to the spontaneous condition, we ran this experiment at contrast levels of 25% and 100%.

The amplitude data as a function of distance was fitted by the equation $M \exp\left(\frac{-d}{\lambda}\right)+B$, with d representing cortical distance and M, B and λ being parameters (with λ being the space constant, M being the magnitude and B being a baseline amplitude). For each condition, we first fitted the equation in the driven condition, as they usually showed a clear saturation level (**Fig. 2a**). The baseline that we obtained from this fit was then fixed and the equation was fitted again for the spontaneous and low-contrast conditions. The time to peak data as a function of distance was fitted with $\frac{d}{v}$, where v represents the propagation speed of the wave. For the distribution of velocities, we selected those cases where the correlation between the measured time to peak and distance achieved a significance level of 0.001, resulting in $n = 83$ electrodes in monkey and $n = 84$ in cat. For the magnitudes, we restricted the analyses to those cases where the exponential fits accounted for more than 50% of the variance, resulting in $n = 116$ electrodes in monkey and $n = 99$ in cat.

Note: Supplementary information is available on the Nature Neuroscience website.

ACKNOWLEDGMENTS

We are grateful to B. Malone, A. Benucci and S. Katzner for help with data collection and valuable discussions. This work was supported by grants from the US National Institutes of Health (EY-17396 to M.C., EY-12816 and EY-18322 to D.L.R.) and DARPA (FA8650-06-C-7633 to D.L.R.), an Oppenheimer/Stein Endowment Award (D.L.R.), a Scholar Award from the McKnight Endowment Fund for Neuroscience (M.C.) and a Leopoldina fellowship (BMBF-LPD9901/8-165 to L.B.). M.C. holds the GlaxoSmithKline/Fight for Sight Chair in Visual Neuroscience.

AUTHOR CONTRIBUTIONS

All authors contributed in the execution of the experiments, the analysis of the data and the writing of the manuscript.

Published online at http://www.nature.com/natureneuroscience/
Reprints and permissions information is available online at http://npg.nature.com/reprintsandpermissions/

1. Reid, R.C. & Alonso, J.M. Specificity of monosynaptic connections from thalamus to visual cortex. *Nature* **378**, 281–284 (1995).
2. Priebe, N.J. & Ferster, D. Inhibition, spike threshold and stimulus selectivity in primary visual cortex. *Neuron* **57**, 482–497 (2008).
3. Ferster, D., Chung, S. & Wheat, H. Orientation selectivity of thalamic input to simple cells of cat visual cortex. *Nature* **380**, 249–252 (1996).
4. Ferster, D. & Miller, K.D. Neural mechanisms of orientation selectivity in the visual cortex. *Annu. Rev. Neurosci.* **23**, 441–471 (2000).
5. Chung, S. & Ferster, D. Strength and orientation tuning of the thalamic input to simple cells revealed by electrically evoked cortical suppression. *Neuron* **20**, 1177–1189 (1998).
6. Ringach, D.L., Hawken, M.J. & Shapley, R. Dynamics of orientation tuning in macaque primary visual cortex. *Nature* **387**, 281–284 (1997).
7. Sompolinsky, H. & Shapley, R. New perspectives on the mechanisms for orientation selectivity. *Curr. Opin. Neurobiol.* **7**, 514–522 (1997).
8. Bringuier, V., Chavane, F., Glaeser, L. & Fregnac, Y. Horizontal propagation of visual activity in the synaptic integration field of area 17 neurons. *Science* **283**, 695–699 (1999).
9. Kenet, T., Bibitchkov, D., Tsodyks, M., Grinvald, A. & Arieli, A. Spontaneously emerging cortical representations of visual attributes. *Nature* **425**, 954–956 (2003).
10. Tsodyks, M., Kenet, T., Grinvald, A. & Arieli, A. Linking spontaneous activity of single cortical neurons and the underlying functional architecture. *Science* **286**, 1943–1946 (1999).
11. Allman, J., Miezin, F. & McGuinness, E. Stimulus specific responses from beyond the classical receptive field: neurophysiological mechanisms for local-global comparisons in visual neurons. *Annu. Rev. Neurosci.* **8**, 407–430 (1985).
12. Levitt, J.B. & Lund, J.S. Contrast dependence of contextual effects in primate visual cortex. *Nature* **387**, 73–76 (1997).
13. Angelucci, A. *et al.* Circuits for local and global signal integration in primary visual cortex. *J. Neurosci.* **22**, 8633–8646 (2002).
14. Jin, J.Z. *et al.* On and off domains of geniculate afferents in cat primary visual cortex. *Nat. Neurosci.* **11**, 88–94 (2008).
15. Katzner, S. *et al.* Local origin of field potentials in visual cortex. *Neuron* (in the press).
16. Kitano, M., Niiyama, K., Kasamatsu, T., Sutter, E.E. & Norcia, A.M. Retinotopic and nonretinotopic field potentials in cat visual cortex. *Vis. Neurosci.* **11**, 953–977 (1994).
17. Benucci, A., Frazor, R.A. & Carandini, M. Standing waves and traveling waves distinguish two circuits in visual cortex. *Neuron* **55**, 103–117 (2007).
18. Grinvald, A., Lieke, E.E., Frostig, R.D. & Hildesheim, R. Cortical point-spread function and long-range lateral interactions revealed by real-time optical imaging of macaque monkey primary visual cortex. *J. Neurosci.* **14**, 2545–2568 (1994).
19. Gilbert, C.D. & Wiesel, T.N. Clustered intrinsic connections in cat visual cortex. *J. Neurosci.* **3**, 1116–1133 (1983).
20. Hirsch, J.A. & Gilbert, C.D. Synaptic physiology of horizontal connections in the cats' visual cortex. *J. Neurosci.* **11**, 1800–1809 (1991).
21. Bosking, W.H., Zhang, Y., Schofield, B. & Fitzpatrick, D. Orientation selectivity and the arrangement of horizontal connections in tree shrew striate cortex. *J. Neurosci.* **17**, 2112–2127 (1997).
22. Nowak, L.G., Munk, M.H., James, A.C., Girard, P. & Bullier, J. Cross-correlation study of the temporal interactions between areas V1 and V2 of the macaque monkey. *J. Neurophysiol.* **81**, 1057–1074 (1999).
23. Song, S., Sjöström, P.J., Reigl, M., Nelson, S. & Chklovskii, D.B. Highly nonrandom features of synaptic connectivity in local cortical circuits. *PLoS Biol.* **3**, e68 (2005).
24. de la Rocha, J., Doiron, B., Shea-Brown, E., Josic, K. & Reyes, A. Correlation between neural spike trains increases with firing rate. *Nature* **448**, 802–806 (2007).
25. Dorn, J.D. & Ringach, D.L. Estimating membrane voltage correlations from extracellular spike trains. *J. Neurophysiol.* **89**, 2271–2278 (2003).
26. Aertsen, A.M. & Gerstein, G.L. Evaluation of neuronal connectivity: sensitivity of cross-correlation. *Brain Res.* **340**, 341–354 (1985).
27. Hoffman, K.P. & Stone, J. Conduction velocity of afferents to cat visual cortex: a correlation with cortical receptive field properties. *Brain Res.* **32**, 460–466 (1971).
28. Lampl, I., Reichova, I. & Ferster, D. Synchronous membrane potential fluctuations in neurons of the cat visual cortex. *Neuron* **22**, 361–374 (1999).
29. Shapley, R., Hawken, M. & Ringach, D.L. Dynamic's of orientation selectivity in the primary visual cortex and the importance of cortical inhibition. *Neuron* **38**, 689–699 (2003).
30. Sceniak, M.P., Ringach, D.L., Hawken, M.J. & Shapley, R. Contrast's effect on spatial summation by macaque V1 neurons. *Nat. Neurosci.* **2**, 733–739 (1999).
31. Cavanaugh, J.R., Bair, W. & Movshon, J.A. Nature and interaction of signals from the receptive field center and surround in macaque V1 neurons. *J. Neurophysiol.* **88**, 2530–2546 (2002).
32. Polat, U., Mizobe, K., Pettet, M.W., Kasamatsu, T. & Norcia, A.M. Collinear stimuli regulate visual responses depending on cell's contrast threshold. *Nature* **391**, 580–584 (1998).
33. Kohn, A. & Smith, M.A. Stimulus dependence of neuronal correlation in primary visual cortex of the macaque. *J. Neurosci.* **25**, 3661–3673 (2005).
34. Finn, I.M., Priebe, N.J. & Ferster, D. The emergence of contrast-invariant orientation tuning in simple cells of cat visual cortex. *Neuron* **54**, 137–152 (2007).
35. Chen, Y., Geisler, W.S. & Seidemann, E. Optimal decoding of correlated neural population responses in the primate visual cortex. *Nat. Neurosci.* **9**, 1412–1420 (2006).
36. Bernander, O., Douglas, R.J., Martin, K.A. & Koch, C. Synaptic background activity influences spatiotemporal integration in single pyramidal cells. *Proc. Natl. Acad. Sci. USA* **88**, 11569–11573 (1991).
37. Destexhe, A. & Pare, D. Impact of network activity on the integrative properties of neocortical pyramidal neurons in vivo. *J. Neurophysiol.* **81**, 1531–1547 (1999).
38. Weliky, M., Kandler, K., Fitzpatrick, D. & Katz, L.C. Patterns of excitation and inhibition evoked by horizontal connections in visual cortex share a common relationship to orientation columns. *Neuron* **15**, 541–552 (1995).
39. Douglas, R.J. & Martin, K.A. Recurrent neuronal circuits in the neocortex. *Curr. Biol.* **17**, R496–R500 (2007).